Chinese Chemical Letters 33 (2022) 1331–1336

Contents lists available at ScienceDirect

Chinese Chemical Letters

journal homepage: www.elsevier.com/locate/cclet

In situ synthesis of red fluorescent gold nanoclusters with enzyme-like activity for oxidative stress amplification in chemodynamic therapy

Wenying Mi, Shuang Tang, Shaoshi Guo, Hejing Li, Na Shao*

College of Chemistry, Beijing Normal University, Beijing 100875, China

ARTICLE INFO

Article history:
Received 31 May 2021
Revised 15 July 2021
Accepted 31 July 2021
Available online 8 August 2021

Keywords:
Chemodynamic therapy
In situ synthesis
Gold nanoclusters
Superoxidase dismutase and peroxidase (POD)-like activity
Oxidative stress amplification

ABSTRACT

Chemodynamic therapy (CDT) has attracted tremendous interest in cancer therapy because it is independent of oxygen and photoirradiation. However, the therapeutic efficacy of CDT is restricted by insufficient H_2O_2 levels in tumor cells. Herein, employing endogenous GSH as a template and cationic polymeric chitosan (CS) as crosslinker and stabilizer exhibiting easy cell uptake, red luminescent gold nanoclusters (denoted CS-GSH@AuNCs) were successfully synthesized in HeLa cells. The *in situ* synthesized CS-GSH@AuNCs exhibited both superoxidase dismutase (SOD) and peroxidase (POD)-like activity, which could promote the production of H_2O_2 from superoxide anion radicals ($O_2^{\bullet-}$) and then $^{\bullet}OH$. The combination of GSH elimination and H_2O_2 elevation boosted the generation of $^{\bullet}OH$, which could trigger cancer cell apoptosis and death. The enzyme-like activity of CS-GSH@AuNCs could be effectively activated under acidic conditions, and showed a high killing effect on tumor cells but minimal toxicity to normal cells. The developed GSH consumption and $^{\bullet}OH$ promotion theranostic platform is an innovative route for enhanced CDT by the amplification of oxidative stress.

Chemodynamic therapy (CDT) is an emerging cancer treatment modality that converts H_2O_2 to $^{\bullet}OH$ *via* Fenton or Fenton-like reactions [1-3]. $^{\bullet}OH$ is the most toxic reactive oxygen species (ROS) that can induce DNA and protein damage as well as liposome peroxidation, leading to cell apoptosis and inhibiting tumor growth [4-6]. Compared with photodynamic therapy (PDT), a therapeutic strategy based on ROS, CDT can prevent the resistance of the hypoxic microenvironment and limit the light penetration depth of solid tumors [7,8]. In addition, Fenton-type reactions can be activated effectively in tumor microenvironments (TMEs) with low pH and high levels of H_2O_2, making CDT minimally harmful to normal tissue [9]. Various nanomaterials with the ability to deliver Fenton-type catalysts have been developed for application in CDT, such as ferrocene [10], iron nanoparticles [11], iron oxide nanoparticles [12] and other metals [13-15]. Since the essence of CDT is to catalyze H_2O_2 to highly toxic $^{\bullet}OH$ and induce tumor cell apoptosis, its therapeutic efficacy largely relies on H_2O_2 levels. Although the concentration of H_2O_2 in tumor cells is far higher than that in normal cells, CDT has difficulty generating enough $^{\bullet}OH$ to achieve satisfactory therapeutic performance [16]. Moreover, the levels of antioxidants (such as GSH) also increases in tumor cells to counterbalance the overproduction of ROS, which largely decreases the cell killing effect of ROS [17, 18].

Enhancing intracellular H_2O_2 levels can be realized by delivering exogenous H_2O_2 or promoting the production of endogenous H_2O_2. Both will cause the ROS level to greatly exceed the antioxidant capacity, known as amplification of oxidative stress. For example, glucose oxidase combined with Fenton nanocatalysts has been reported to elevate H_2O_2 concentration via enzyme-catalyzed reaction of glucose, which is overexpressed in tumor cells due to their active metabolism [19,20]. Metal peroxides, which possess pH-dependent H_2O_2 release capacity, were also used to achieve high efficiency CDT by elevating H_2O_2 levels in tumors [14,16,21]. Lin *et al.* synthesized copper peroxide nanodots and utilized them to enhance CDT by H_2O_2 self-supply [16].

On the other hand, amplifying the production of ROS can be realized by depleting endogenous GSH or inhibiting the generation of GSH [22,23]. For instance, nanocarriers coated with ferrous nanocomplexs as Fenton catalysts and L-buthionine sulfoximine (BSO) as a GSH inhibitor were applied for oxidative stress-enhanced CDT and radiotherapy [24]. Because Au could bind sulfhydryls by forming Au-S bonds, Au-containing nanomaterials have been used as GSH-depleting agents to achieve oxidative stress amplification in tumor cells [25-27]. Jointly promoting H_2O_2 production and GSH consumption is an effective strategy to enhance the anticancer efficacy of CDT agents [28,29]. Developing simple

* Corresponding author.
E-mail address: shaona@bnu.edu.cn (N. Shao).

https://doi.org/10.1016/j.cclet.2021.07.073
1001-8417/

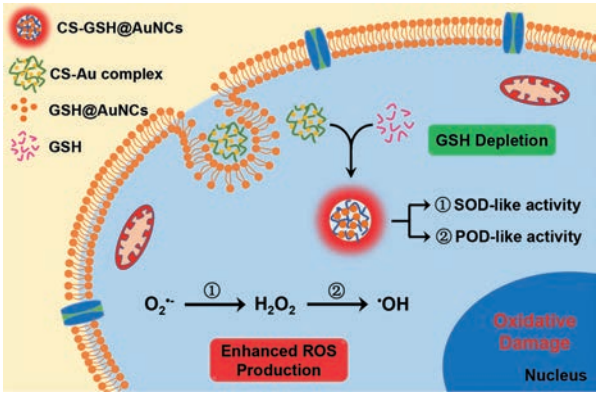

Scheme 1. Illustration of the *in situ* synthesis of CS-GSH@AuNCs and their application in chemodynamic therapy.

but efficient CDT agents by promoting the production of H_2O_2 and elimination of GSH is of great significance.

GSH is a common functional substance regulating redox balance in organisms, especially at a high concentration of 1–10 mmol/L in tumor cells [30]. GSH is the most commonly used ligand for the synthesis of metal nanoclusters (MNCs), which have been widely applied in biosensing, bioimaging and biocatalysis [31-33], due to their excellent biocompatibility, facile synthesis and low biotoxicity. Endogenous GSH has been used as a template to synthesize MNCs in cells or tissue, known as *in situ* synthesis [34-37]. However, most of in situ synthesized MNCs emit blue or green fluorescence, of which the signal is susceptible to interference by the background fluorescence or cell autofluorescence. In addition, almost all studies have focused on the biosensing of GSH or biolabeling of cancer cells, and few have examined the application of GSH-MNCs in cancer treatment by amplification of oxidative stress *via* GSH depletion.

In this study, utilizing biocompatible chitosan (CS) as a stabilizer [38], *in situ* synthesis of red fluorescent CS-GSH@AuNCs was realized in cancer cells by consumption of endogenous GSH. More importantly, the synthesized CS-GSH@AuNCs exhibited both SOD and POD-like activity, which can catalyze $O_2^{\bullet-}$ to H_2O_2, and further to $^{\bullet}OH$, and could be used to enhance CDT by depleting GSH and in turn facilitating H_2O_2/$^{\bullet}OH$ production (Scheme 1). The CS-GSH@AuNCs showed high cytotoxicity toward HeLa cells but little harm to normal cells. The anticancer CDT efficacy of the synthesized CS-GSH@AuNCs was proven *in vitro* by MTT assay, calcein AM/PI costaining assay and flow cytometric analysis, and the results demonstrated that the CS-GSH@AuNCs had good cancer cell killing effects.

GSH is a common template for the synthesis of gold nanoclusters owing to the strong binding interactions between Au and S [39]. However, most GSH-templated gold nanoclusters were prepared at high temperature or in the presence of a strong reductant to achieve acceptable stability and luminescence [40,41]. It was reported that chitosan (CS) could induce significant luminescence enhancement of GSH@AuNCs *via* self-assembly [42,43]. Thus, we expected that mild synthesis conditions might be achieved if CS was introduced with GSH and $HAuCl_4$ during the synthesis of GSH@AuNCs. The results showed that CS-GSH@AuNCs with strong red luminescence were successfully prepared at room temperature and without the addition of extra reductant. The optimization of the molar ratio of Au to GSH (Au/GSH), pH and content of CS for the synthesis of CS-GSH@AuNCs in solution is shown in Fig. S1 (Supporting information).

XPS analysis (Fig. 1A) showed the existence of Au(0) and Au(I) in CS-GSH@AuNCs, with contents of 72.94% and 27.06%, respectively. The optical properties of the as prepared CS-GSH@AuNCs were investigated. As shown in Fig. 1B, CS-GSH@AuNCs showed a maximum emission peak at 625 nm with an absolute quantum yield of 8.1% when excited at 370 nm. The UV-visible absorption spectrum showed no obvious plasma scattering peak ranging from 450 nm to 650 nm appeared (Fig. 1C), which is consistent with the UV-visible absorption characteristics of most GSH-templated nanoclusters [44,45]. These results indicated the formation of AuNCs. For comparison, GSH@AuNCs and CS-$HAuCl_4$ complexes were prepared under similar conditions as those for CS-GSH@AuNCs. As shown in Fig. 1D, GSH@AuNCs showed weak emission ranging from 500 nm to 720 nm, and the CS-$HAuCl_4$ complex had no emission peak from 500 nm to 720 nm, while the fluorescence intensity of CS-GSH@AuNCs increased approximately 7.6 times compared with that of GSH@AuNCs. This result indicated that the introduction of CS enhanced the fluorescence intensity of GSH@AuNCs. TEM images depicted that CS-GSH@AuNCs had a net-like structure at low resolution (Fig. 1E), and were composed of smaller spherical particles at high resolution (Fig. 1F). GSH@AuNCs showed high dispersity at either low or high resolution (Fig. S2 in Supporting information). The individual AuNCs in CS-GSH@AuNCs had a diameter of 2.04 nm as GSH@AuNCs, with a diameter of 1.90 nm (Fig. S3 in Supporting information).

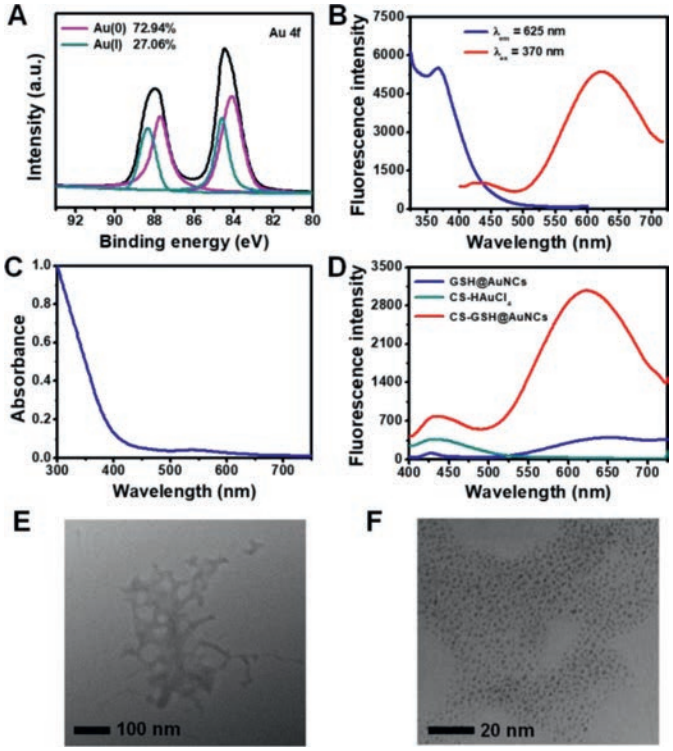

Fig. 1. (A) XPS analysis of Au element in the CS-GSH@AuNCs. Fluorescent excitation and emission spectra (B) and UV-visible absorption spectra (C) of CS-GSH@AuNCs. (D) Fluorescence spectra of GSH@AuNCs, CS-GSH@AuNCs, and the mixture of $HAuCl_4$ and CS. TEM images of CS-GSH@AuNCs at low resolution (E) and high resolution (F).

To further explore the role of CS in the synthesized CS-GSH@AuNCs, the hydrodynamic diameter and zeta potential of GSH@AuNCs and CS-GSH@AuNCs were determined. As shown in Figs. 2A and B, CS-GSH@AuNCs showed a narrow particle size distribution and the hydrodynamic diameter increased to 355 nm from 57 nm compared with that of GSH@AuNCs. The zeta potential of GSH@AuNCs was approximately −68.4 mV (Fig. 2C), implying that GSH@AuNCs had a negative surface charge, which was consistent with the literature [43]. While the zeta potential of CS-

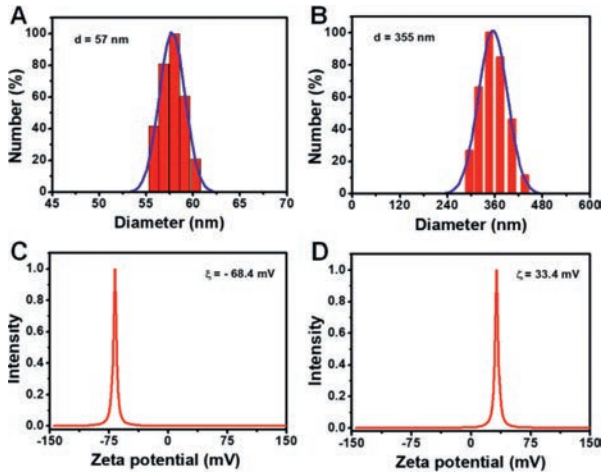

Fig. 2. Hydrodynamic diameter of GSH@AuNCs (A) and CS-GSH@AuNCs (B). Zeta potential measurements of GSH@AuNCs (C) and CS-GSH@AuNCs (D).

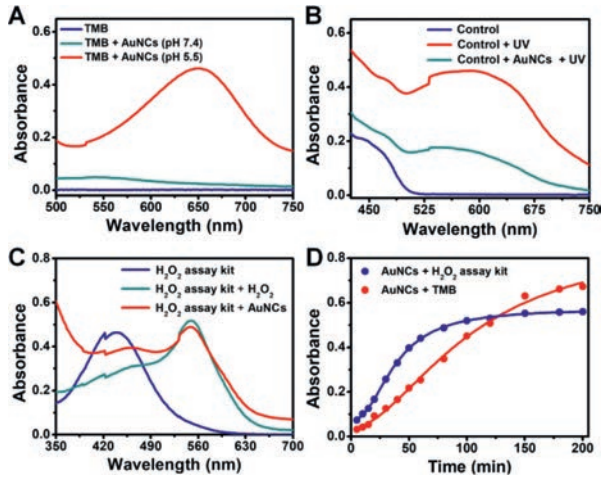

Fig. 3. (A) UV-visible absorption spectra of TMB without and with CS-GSH@AuNCs. (B) SOD-like activity measurement by NBT chromogenic method, the control refers to the mixture solution of riboflavin (200 μmol/L), methionine (130 mmol/L) and NBT (750 μmol/L). (C) H_2O_2-generation determination *via* commercial H_2O_2 analyzer. (D) The changes of the production of H_2O_2 and $^{\bullet}OH$ with time.

GSH@AuNCs was approximately 33.5 mV (Fig. 2D), and these materials were positively charged. It was considered that the negatively charged GSH@AuNCs were connected with the cationic polymer CS *via* electrostatic interactions by forming a framework structure, and the nonradiative transitions of the excited electrons associated with the surface ligand were inhibited, thus leading to fluorescence enhancement of CS-GSH@AuNCs [43,46]. In addition, the combination of GSH@AuNCs with CS improved the stability of AuNCs, which enabled CS-GSH@AuNCs to be synthesized under mild conditions.

It has been reported that AuNCs can function as peroxidase (POD)-like catalysts to decompose H_2O_2 into $^{\bullet}OH$, which in turn could oxidize chromogenic substrates providing a colorimetric measurement [47,48]. Here, the POD-like activity of CS-GSH@AuNCs was assessed by a colorimetric assay with 3,3′,5,5′-tetramethylbenzidine (TMB) as a chromogenic substrate. As shown in Fig. S4 (Supporting information), CS-GSH@AuNCs could induce an apparent color change of TMB from colorless to blue-green under acidic conditions, with a distinct absorption peak at 650 nm (Fig. 3A), but without any change under neutral conditions, indicating that CS-GSH@AuNCs possess POD-like activity.

However, the catalytic oxidation reaction between CS-GSH@AuNCs and TMB did not involve exogenous H_2O_2. We hypothesized that CS-GSH@AuNCs should have superoxide dismutase (SOD)-like activity which could convert superoxide anion radicals ($O_2^{\bullet-}$) coming from dissolved oxygen to H_2O_2. Thus the classic nitroblue tetrazolium (NBT) chromogenic method was employed to evaluate the SOD-like activity of CS-GSH@AuNCs. As shown in Fig. 3B, in the absence of CS-GSH@AuNCs, the solution of riboflavin and methionine could produce $O_2^{\bullet-}$ upon UV irradiation, which could oxidize NBT to blue formazan with a distinct absorption peak at 560 nm. The absorption peak at 560 nm decreased remarkably in intensity after CS-GSH@AuNCs were added, implying that the produced $O_2^{\bullet-}$ should be eliminated by the CS-GSH@AuNCs. Then, an H_2O_2 quantitative assay kit was utilized to further determine the generation of H_2O_2. As shown in Fig. 3C, once H_2O_2 or CS-GSH@AuNCs were introduced into the H_2O_2 assay reagent, the absorption peak at 440 nm decreased in intensity, and a new significant peak at 550 nm appeared, indicating that our CS-GSH@AuNCs could produce H_2O_2. Taking the absorbance of the assay kit solution with CS-GSH@AuNCs added at 550 nm as the H_2O_2-generation capacity (Fig. S5A in Supporting information) and the absorbance of the TMB solution with CS-GSH@AuNCs added at 650 nm as the $^{\bullet}OH$-generation capacity (Fig. S5B in Supporting information), the dynamic process of H_2O_2 and $^{\bullet}OH$ production by CS-GSH@AuNCs under acidic conditions was investigated. As shown in Fig. 3D, the production of H_2O_2 increased rapidly and tended to be balanced after 100 min. The production of $^{\bullet}OH$ increased relatively moderately and slightly decreased after 120 min. The results confirmed the enzymatic characteristics of CS-GSH@AuNCs, meaning that $O_2^{\bullet-}$ was catalyzed to H_2O_2 by SOD-like activity, and the produced H_2O_2 was further catalyzed into $^{\bullet}OH$ by POD-like activity.

To clarify that the color change of TMB was attributed to the SOD and POD-like activity of CS-GSH@AuNCs rather than to oxidase-like activity, *p*-benzoquinone and TBA were used to mask $O_2^{\bullet-}$ and $^{\bullet}OH$, respectively. As shown in Fig S8 (Supporting information), a significant absorption peak appeared at approximately 560 nm when TMB was added into CS-GSH@AuNCs under acidic conditions, but no absorption peak was observed when $O_2^{\bullet-}$ and $^{\bullet}OH$ were masked in advance. Meanwhile, the dissolved oxygen in the solution of TMB and CS-GSH@AuNCs was removed by passing nitrogen to eliminate the oxidase-like activity of CS-GSH@AuNCs. As shown in Fig. S7 (Supporting information), oxygen had no effect on the catalytic reaction between CS-GSH@AuNCs and TMB. These results indicated that CS-GSH@AuNCs possess SOD and POD-like activity but do not possess oxidase-like activity.

Although significant progress has been made in controlling the growth of AuNCs in solution, the *in situ* growth of AuNCs was restricted by harsh conditions such as high temperature or the presence of a strong reductant. Considering that the conditions used to synthesize our CS-GSH@AuNCs were close to physiological conditions, the intracellular GSH content was high, and the cationic polymer CS was good for cell uptake and low biotoxicity, the synthesis of CS-GSH@AuNCs was realized in HeLa cells. First, the effect of other commonly existing biomolecules and ions on the synthesis of CS-GSH@AuNCs was investigated *in vitro*. As shown in Fig. S8 (Supporting information), only GSH could induce significant fluorescence after incubation with CS-$HAuCl_4$, even though BSA and Cys showed weak fluorescence after treatment with CS-$HAuCl_4$. The results demonstrated that the biomolecules and ions common in cells should have little effect on the *in situ* synthesis of CS-GSH@ AuNCs. Then, CS-GSH@AuNCs were biosynthesized in HeLa cells by incubating cells with CS-$HAuCl_4$. As shown in Fig. 4, the cells emitted red fluorescence after incubation with CS-$HAuCl_4$ for 24 h, and the fluorescence signal was enhanced with increasing incubation time. The result indicated that red fluorescent CS-

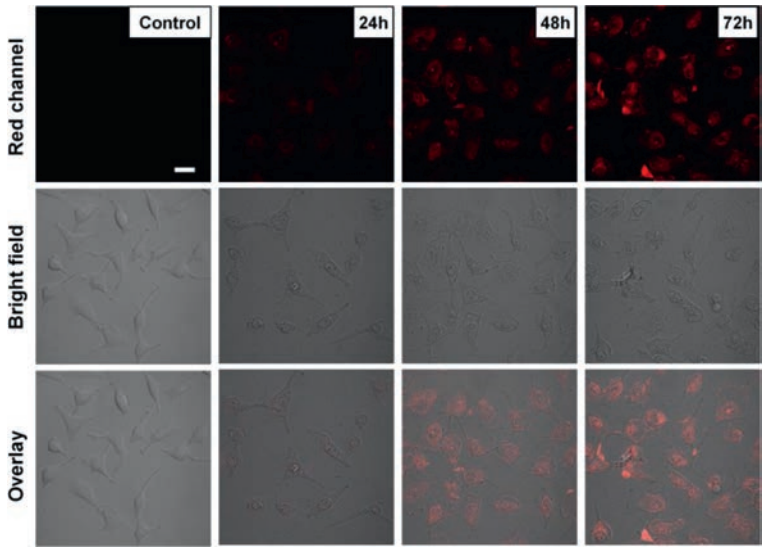

Fig. 4. Fluorescence confocal microscopy images of Hela cells alone (the line of control), and cells treated with CS-$HAuCl_4$ incubated for 24-72 h (The scale bar is 20 μm).

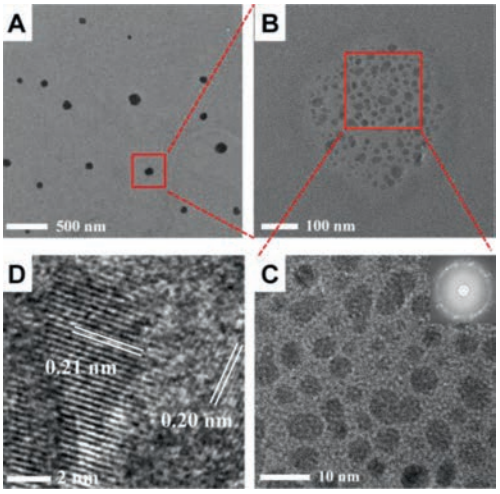

Fig. 5. TEM images of biosynthesized CS-GSH@AuNCs in HeLa cells under different magnification.

GSH@AuNCs were successfully synthesized in cells. NAC as a promoter for the generation of intracellular GSH, was used to verify that the red fluorescence came from the reactions between intracellular GSH and CS-$HAuCl_4$. As shown in Fig. S9 (Supporting information), cells pretreated with NAC for 30 min before incubation with CS-$HAuCl_4$ exhibited an enhanced fluorescence signal, implying the interactions of CS-$HAuCl_4$ with endogenous GSH to form fluorescent CS-GSH@AuNCs.

The intracellular presence of biosynthesized CS-GSH@AuNCs was confirmed by TEM tests. As shown in Fig. 5A, spherical CS-GSH@AuNCs with an average diameter of 90.6 nm (Fig. S10A in Supporting information) were clearly observed in the TEM images, and the individual GSH@AuNCs could be identified in high-resolution TEM images (Figs. 5B and C), with an average diameter of 3.0 nm (Fig. S10B in Supporting information). The diffraction pattern (the insert of Fig. 5C) and the interplanar spacing of 0.21 nm and 0.20 nm (Fig. 5D) confirm the presence of AuNCs. The size of individual AuNCs in the CS-GSH@AuNCs increased from *ca.* 2.0 nm synthesized in solution to 3.0 nm for the intracellular synthesized one should be mainly attributed to the different pH, temperature, incubation time and matter content of GSH and CS-$HAuCl_4$. pH away from the isoelectric point of CS and GSH, higher temperature, longer incubation time and lower concentration of GSH as well as CS-$HAuCl_4$ would give rise to the formation of larger size nanoclusters.

Superoxide anions ($O_2^{\bullet-}$) generated from NADPH oxidases (NOXs) and mitochondrial electron transport chains (ETCs) serve as the main sources of H_2O_2 in living systems, and the overall cellular concentration of $O_2^{\bullet-}$ is maintained at approximately 10^{-11} mol/L [6,49]. The biosynthesized CS-GSH@AuNCs with SOD and POD-like activity would promote the conversion of $O_2^{\bullet-}$ to H_2O_2, and then to $^{\bullet}OH$, leading to the amplification of intracellular oxidative stress. 2,7-Dichlorfluorescin diacetate (DCFH-DA), a nonfluorescent compound that can be efficiently oxidized to fluorescent DCF, was employed as an ROS fluorescent indicator to monitor $^{\bullet}OH$ production. The cells were pretreated with CS-$HAuCl_4$ for 24 h to 72 h and then stained with DCFH-DA for 30 min before fluorescence confocal imaging. As shown in Fig. 6, a green fluorescence signal was observable after the HeLa cells were was incubated with CS-$HAuCl_4$ for 24 h, and the fluorescence signal enhanced as the incubation time increased to 48 and 72 h, while no detectable fluorescence was observed for the control experiment. This demonstrated that the CS-GSH@AuNCs synthesized *in situ* still exhibited enzyme-like catalytic activity, which could elevate intracellular ROS levels. Considering that the optimal pH for preparing CS-GSH@AuNCs in solution was 6.0 and that enzyme-like activity could be efficiently activated under acidic conditions, $^{\bullet}OH$ generation was investigated at different pH. The cells were incubated with CS-$HAuCl_4$ for 72 h at pH 6.0 or 7.4 and then stained with DCFH-DA for 30 min. As shown in Fig. S11 (Supporting information), the cells incubated under acidic conditions exhibited ultrahigh fluorescence signals compared to those incubated under neutral conditions, which was conducive to their role in the tumor microenvironment.

Encouraged by the excellent capacity of the *in situ* synthesized CS-GSH@AuNCs for $^{\bullet}OH$ generation, their CDT efficiency in cells was evaluated. Primarily, the viability of normal cells and cancer cells treated with CS-$HAuCl_4$ was measured by the classic methyl thiazolyl tetrazolium (MTT) assay. CS-$HAuCl_4$ showed dose-dependent cytotoxicity toward cancer cells (*e.g.*, HeLa) (Fig. 7A), blue bar), and the cell viability was 50% when the concentration of Au was 250 μmol/L. CS-$HAuCl_4$ presented relatively low cytotoxicity toward normal cells (*e.g.*, 293-T) even though the concentration of Au reached 250 μmol/L, with a cell viability of 90% (Fig. 7B). This should be attributed to the higher GSH level in cancer cells

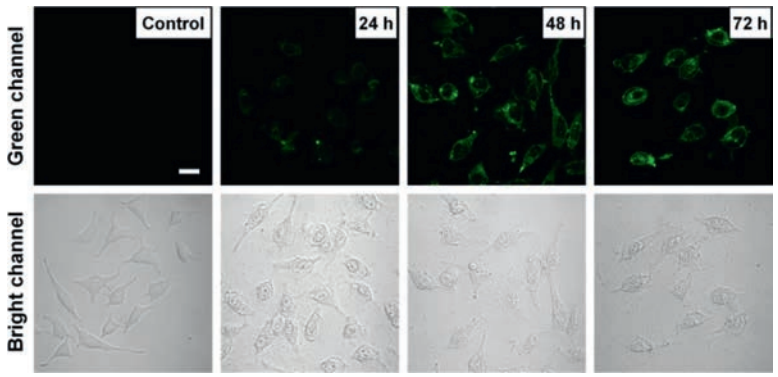

Fig. 6. Fluorescence confocal microscopy images of HeLa cells only stained with DCFH-DA (the line of control), and cells incubated with CS-$HAuCl_4$ for 24-72 h before staining with DCFH-DA (the scale bar is 20 μm).

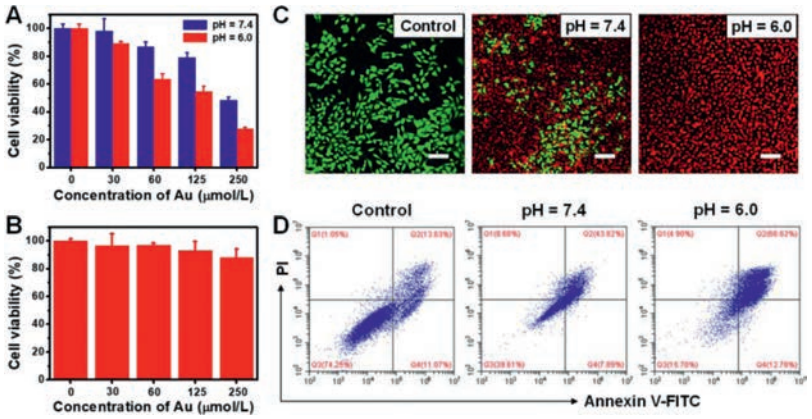

Fig. 7. (A) Cell viability of HeLa cells treated with CS-$HAuCl_4$ for 48 h under different pH. (B) Cell viability of 293-T cells after incubation with CS-$HAuCl_4$ for 48 h at pH 7.4. (C) Fluorescence confocal images of HeLa cells costained with calcein AM (green, live cells) and PI (red, dead cells) after incubation without (control) or with CS-$HAuCl_4$ for 48 h (the concentration of Au was 250 μmol/L, the scale bar is 100 μm). (D) Flow cytometry analysis of HeLa cell apoptosis after treatment without (control) or with CS-$HAuCl_4$ for 48 h.

than in normal cells, which was beneficial for the formation of CS-GSH@AuNCs. To simulate the moderately acidic tumor microenvironment, the cell viability of HeLa cells treated with CS-$HAuCl_4$ at pH 6.0 was evaluated, and it showed a more significant dose dependence with the cell viability decreasing to 30% when the Au concentration was 250 μmol/L (Fig. 7A, red bar). These results suggested that the cell killing effect could be efficiently triggered in an acidic tumor environment. The ability of CS-GSH@AuNCs to induce the death of cancer cells was further explored by a live/dead cell staining assay. As depicted by fluorescence images of calcein AM- and propidium (PI)- costained HeLa cells (Fig. S12 in Supporting information), the *in situ* synthesized CS-GSH@AuNCs induced cell death in a dose-dependent manner. As anticipated, cells incubated with CS-$HAuCl_4$ displayed a higher CDT efficacy at pH 6.0 than at pH 7.4 (Fig. 7C). Furthermore, flow cytometry analysis in which cells were stained with annexin V-FITC and PI revealed a high percentage of apoptotic HeLa cells treated with CS-$HAuCl_4$ compared with the control experiment, and the cell apoptosis rate greatly increased under weakly acidic conditions (Fig. 7D). The study demonstrated that enhanced cytotoxicity to induce cancer cell death could be achieved by controlling CS-GSH@AuNCs growth in cells, which amplified intracellular oxidative stress by consuming endogenous GSH as well as producing H_2O_2 and $^{\bullet}OH$, suggesting the potential of using in situ synthesized CS-GSH@AuNCs for highly efficient CDT.

In summary, we reported the biosynthesis of CS-GSH@AuNCs in HeLa cells and their application as CDT agents *via* oxidative stress amplification. Red fluorescent CS-GSH@AuNCs could be synthesized in cancer cells utilizing endogenous GSH by treating cells with CS-$HAuCl_4$, and the prepared CS-GSH@AuNCs exhibited SOD and POD-like activity that could catalyze $O_2^{\bullet-}$ into H_2O_2 and further to $^{\bullet}OH$. The in situ synthesized CS-GSH@AuNCs could significantly amplify intracellular oxidative stress under acidic conditions by combining GSH depletion and $^{\bullet}OH$ production, and displayed enhanced cell killing capacity for cancer cells *via* CDT with negligible toxicity to normal cells. This work provides a new strategy for cancer treatment with CDT by controlling AuNCs growth in the tumor microenvironment.

Declaration of competing interest

The authors declare that they have no known competing financial interests or personal relationships that could have appeared to influence the work reported in this paper.

Acknowledgment

The project was supported by the National Natural Science Foundation of China (No. 22074007).

Supplementary materials

Supplementary material associated with this article can be found, in the online version, at doi:10.1016/j.cclet.2021.07.073.

References

[1] Z. Tang, Y. Liu, M. He, W. Bu, Angew. Chem. 58 (2019) 946–956.
[2] X. Wang, X. Zhong, Z. Liu, L. Cheng, Nano Today 35 (2020) 100946.
[3] E. Hwang, H.S. Jung, Chem. Commun. 56 (2020) 8332–8341.
[4] J.N. Moloney, T.G. Cotter, Semin. Cell. Dev. Biol. 80 (2018) 50–64.
[5] X.Q. Wang, W. Wang, M. Peng, X.Z. Zhang, Biomaterials 266 (2021) 120474.
[6] H. Sies, D.P. Jones, Nat. Rev. Mol. Cell Biol. 21 (2020) 363–383.
[7] Y. Cai, D. Ni, W. Cheng, et al., Angew. Chem. Int. Ed. 59 (2020) 14014–14018.
[8] Y. He, S. Hua Liu, J. Yin, J. Yoon, Coord. Chem. Rev. 429 (2021) 213610.
[9] F. Gong, N. Yang, X. Wang, et al., Nano Today 32 (2020) 100851.
[10] P. Zhao, Z. Tang, X. Chen, et al., Mater. Horiz. 6 (2019) 369–374.
[11] C. Zhang, W. Bu, D. Ni, et al., Angew. Chem. Int. Ed. 55 (2016) 2101–2106.
[12] X. Liu, Y. Liu, J. Wang, T. Wei, Z. Dai, ACS Appl. Mater. Interfaces. 11 (2019) 23065–23071.
[13] B. Ma, S. Wang, F. Liu, et al., J. Am. Chem. Soc. 141 (2019) 849–857.
[14] Y. Sang, F. Cao, W. Li, et al., J. Am. Chem. Soc. 142 (2020) 5177–5183.
[15] S. Cao, J. Fan, W. Sun, et al., Chem. Commun. 55 (2019) 12956–12959.
[16] L.S. Lin, T. Huang, J. Song, et al., J. Am. Chem. Soc. 141 (2019) 9937–9945.
[17] X. Zhong, X. Wang, L. Cheng, et al., Adv. Funct. Mater. 30 (2019) 1907954.
[18] Z. Qing, A. Bai, L. Chen, et al., CCS Chem. 3 (2021) 1217–1230.
[19] M. Huo, L. Wang, Y. Chen, J. Shi, Nat. Commun. 8 (2017) 357.
[20] L.H. Fu, Y. Wan, C. Qi, et al., Adv. Mater. 33 (2021) e2006892.
[21] Y. Han, J. Ouyang, Y. Li, F. Wang, J.H. Jiang, ACS Appl. Mater. Interfaces 12 (2019) 288–297.
[22] H. Fan, G. Yan, Z. Zhao, et al., Angew. Chem. Int. Ed. 55 (2016) 5477–5482.
[23] F. Gong, L. Cheng, N. Yang, et al., Adv. Mater. 31 (2019) e1900730.
[24] Z. Dong, L. Feng, Y. Chao, et al., Nano Lett. 19 (2019) 805–815.
[25] N. Gong, X. Ma, X. Ye, et al., Nat. Nanotechnol. 14 (2019) 379–387.
[26] X. Zhang, X. Chen, Y.W. Jiang, et al., ACS Appl. Mater. Interfaces 10 (2018) 10601–10606.
[27] Z.H. Qing, G.Y. Luo, S.H. Xing, et al., Angew. Chem. Int. Ed. 59 (2020) 14044–14048.
[28] M. Chang, M. Wang, M. Wang, et al., Adv. Mater. 31 (2019) e1905271.
[29] H. Tian, M. Zhang, G. Jin, Y. Jiang, Y. Luan, J. Colloid Interface Sci. 587 (2021) 358–366.
[30] G.Y. Wu, Y.Z. Fang, S. Yang, J.R. Lupton, N.D. Turner, J. Nutr. 134 (2004) 489–492.
[31] Z. Qiao, J. Zhang, X. Hai, et al., Biosens. Bioelectron. 176 (2021) 112898.
[32] X. Kang, Y. Li, M. Zhu, R. Jin, Chem. Soc. Rev. 49 (2020) 6443–6514.
[33] T. Higaki, Y. Li, S. Zhao, et al., Angew. Chem. Int. Ed. 58 (2019) 8291–8302.
[34] C. Peng, M. Yu, J. Zheng, Nano Lett. 20 (2020) 1378–1382.
[35] D. Chen, C. Zhao, J. Ye, et al., ACS Appl. Mater. Interfaces 7 (2015) 18163–18169.
[36] A.L. West, N.M. Schaeublin, M.H. Griep, et al., ACS Appl. Mater. Interfaces 8 (2016) 21221–21227.
[37] F. Dong, E. Feng, T. Zheng, Y. Tian, ACS Appl. Mater. Interfaces 10 (2018) 2051–2057.
[38] E. Frohlich, Int. J. Nanomedicine 7 (2012) 5577–5591.
[39] D.E. Jiang, Nanoscale 5 (2013) 7149–7160.
[40] Y. Yu, X. Chen, Q. Yao, et al., Chem. Mater. 25 (2013) 946–952.
[41] J.G. You, C.Y. Lu, A.S. Krishna Kumar, W.L. Tseng, Nanoscale 10 (2018) 17691–17698.
[42] N. Goswami, F. Lin, Y. Liu, D.T. Leong, J. Xie, Chem. Mater. 28 (2016) 4009–4016.
[43] J. Zhu, K. He, Z. Dai, et al., Anal. Chem. 91 (2019) 8237–8243.
[44] X. Xie, Z. Peng, X. Hua, et al., Biosens. Bioelectron. 148 (2020) 111829.
[45] Z. Wang, Z. Zhu, C. Zhao, et al., Chem. Asian J. 14 (2019) 765–769.
[46] N. Goswami, Q. Yao, Z. Luo, et al., J. Phys. Chem. Lett. 7 (2016) 962–975.
[47] C.N. Loynachan, A.P. Soleimany, J.S. Dudani, et al., Nat. Nanotechnol. 14 (2019) 883–890.
[48] C. Chen, D. Zhao, Y. Jiang, et al., Anal. Chem. 91 (2019) 15017–15024.
[49] Y. Wang, R. Branicky, A. Noe, S. Hekimi, J. Cell. Biol. 217 (2018) 1915–1928.